The $1 < z < 5$ Infrared Luminosity Function of Type I Quasars

Michael J. I. Brown[1†], Kate Brand[2], Arjun Dey[2], Buell T. Jannuzi[2], Richard Cool[3], Emeric Le Floc'h[3,4], Christopher S. Kochanek[5], Lee Armus[6], Chao Bian[7], Jim Higdon[8], Sarah Higdon[8], Casey Papovich[3], George Rieke[3], Marcia Rieke[3], J. D. Smith[3], B. T. Soifer[6,7], Dan Weedman[8]

mbrown@astro.princeton.edu

ABSTRACT

We determine the rest-frame 8μm luminosity function of type I quasars over the redshift range $1 < z < 5$. Our sample consists of 292 24μm sources brighter than 1 mJy selected from 7.17 deg^2 of the *Spitzer Space Telescope* MIPS survey of the NOAO Deep Wide-Field Survey Boötes field. The AGN and Galaxy Evolution Survey (AGES) has measured redshifts for 270 of the $R < 21.7$ sources and we estimate that the contamination of the remaining 22 sources by stars and galaxies is low. We are able to select quasars missed by ultra-violet excess quasar surveys, including reddened type I quasars and $2.2 < z < 3.0$ quasars with optical colors similar to main sequence stars. We find reddened type I quasars comprise $\sim 20\%$ of the type I quasar population. Nonetheless, the shape, normalization, and evolution of the rest-frame 8μm luminosity function is comparable to that of quasars selected from optical surveys. The 8 μm luminosity function of type I quasars is well approximated by a power-law with index -2.75 ± 0.14. We directly measure the peak of the quasar space density to be at $z = 2.6 \pm 0.3$.

Subject headings: quasars: general

[1]Princeton University Observatory, Peyton Hall, Princeton, NJ 08544-1001, USA

[2]National Optical Astronomy Observatory, Tucson, AZ 85726-6732, USA

[3]Steward Observatory, University of Arizona, Tucson, AZ 85721, USA

[4]Observatoire de Paris, GEPI, 92195 Meudon, France

[5]Department of Astronomy, The Ohio State University, 140 West 18th Avenue, Columbus, OH 43210, USA

[6]Spitzer Science Center, IPAC, California Institute of Technology, MC 220-6, 1200 East California Boulevard, Pasadena, CA 91125, USA

[7]The Division of Physics, Mathematics & Astronomy, California Institute of Technology, 1200 East California Boulevard, Pasadena, CA 91125, USA

[8]Astronomy Department, Cornell University, Ithaca, NY 14853, USA

[†]H.N. Russell Fellow

1. INTRODUCTION

The luminosity function of Active Galactic Nuclei (AGNs) is one of the principal constraints on the growth of supermassive black holes over the age of the Universe (e.g., Kauffmann & Haehnelt 2000). Ideally, we would measure the bolometric luminosity function of all AGNs as a function of redshift. This is not trivial, as it requires deep multiwavelength data spanning X-ray to submm wavelengths and sampling large comoving volumes. In practice, surveys select subsets of AGNs in relatively narrow wavelength ranges. For example, optical quasar surveys generally select quasars with blue spectral energy distributions and broad emission lines. While using a narrow wavelength range as a proxy for bolometric luminosity would appear risky, this approach seems to have been remarkably successful. Optical, radio, and X-ray luminosity functions of AGNs infer a $z \simeq 2.5$ peak in the space density of the most luminous quasars

(e.g., Dunlop & Peacock 1990; Ueda et al. 2003; Croom et al. 2004). This agreement is reassuring, since the three selection methods have different biases – strong radio emission only occurs in a small subset of all AGNs, optical wavelengths are sensitive to dust absorption, and soft X-ray wavelengths are sensitive to gas absorption.

It is the absorption of radiation by the gas and dust surrounding the black hole that creates the greatest systematic uncertainties. In particular, unified models of AGNs (e.g., Antonucci 1993) assume the presence of obscuring material with a non-isotropic spatial distribution that makes the observed spectrum a function of viewing angle. In unified models of AGNs, the obscuring material is often referred to as the torus, though the actual distribution of gas and dust may be significantly more complex and its properties could depend on luminosity, time or Eddington factors (e.g., Lawrence 1991; Hopkins et al. 2005). When AGNs are viewed from above the torus, optical continuum and broad emission lines associated with regions near the central black hole can be observed directly. When AGNs are viewed in the plane of the torus, optical continuum and the broad emission lines are absorbed.

Selection biases due to absorption by dust or gas are minimized by selecting AGNs in the infrared. In this paper we combine *Spitzer Space Telescope* 24 μm imaging of the Boötes field (Rieke et al. 2004; Houck et al. 2005) of the optical NOAO Deep Wide-Field Survey (NDWFS; Jannuzi & Dey 1999), with spectroscopy of quasar candidates by the AGN and Galaxy Evolution Survey (AGES, Kochanek et al. in preparation) to determine the rest-frame 8 μm luminosity function of type I quasars. This allows us to identify quasars that would be missed in optical surveys either because of extinction or because the quasars have optical colors typical of main sequence stars.

The structure of this paper is as follows. In §2 we describe the surveys used to produce the quasar sample. In §3 we characterize the sample, discuss its completeness and compare it to other selection methods available for the field. In §4 we derive the luminosity function of the type I quasars in the sample, and in §5 we discuss the role of type II quasars. We summarize our results and discuss future prospects in §6. Throughout this paper we define type I quasars as AGNs with optical and ultraviolet emission lines broader than 1000 km s^{-1} and type II quasars as those with narrower lines. In this paper we adopt a cosmology of $\Omega_m = 0.3$, $\Omega_\Lambda = 0.7$, and $H_0 = 70$ km s^{-1} Mpc. Throughout this paper we use *AB* magnitudes although the released NDWFS, 2MASS, and USNO-A2 catalogs use Vega magnitudes[1].

2. THE SURVEYS

Our sample combines three surveys of Boötes – the NDWFS and *Spitzer* MIPS imaging surveys and the AGES spectroscopic survey. In this section we discuss the general properties of these three surveys and summarize the final multi-wavelength catalog.

2.1. The NOAO Deep Wide-Field Survey

The NDWFS is an optical and near-infrared imaging survey of two $\approx$ 9.3 deg^2 fields with NOAO telescopes (Jannuzi & Dey 1999). In this paper, we utilize the third data release of NDWFS $B_W RI$ imaging of the Boötes field, which is available from the NOAO Science Archive[2]. A thorough description of the optical observing strategy and data reduction will be provided by Jannuzi et al. (in preparation).

Object catalogs were generated using SExtractor 2.3.2 (Bertin & Arnouts 1996) run in single-image mode. Detections in the different bands were matched if the centroids were within 1″ of each other. For extended objects, detections in the different bands were matched if the centroid in one band was within an ellipse defined using the second order moments of the light distribution of the object in another band[3]. Throughout this paper we use SExtractor MAG_AUTO magnitudes (which are similar to Kron total magnitudes; Kron 1980) for optical photometry, due to their small uncertainties and systematic errors at faint magnitudes. The 50% completeness limits of the SExtractor catalogs for point sources are $B_W \simeq 26.5$, $R \simeq 25.5$ and $I \simeq 25.3$.

We used SExtractor's star-galaxy classifier to classify objects as compact or extended. For

[1] $B_{W,AB} = B_{W,\mathrm{Vega}}$, $R_{AB} = R_{\mathrm{Vega}} + 0.20$, $I_{AB} = I_{\mathrm{Vega}} + 0.45$, and $J_{AB} = J_{\mathrm{Vega}} + 0.89$

[2] http://www.archive.noao.edu/ndwfs/

[3] This ellipse was defined with the SExtractor parameters 2 × A_WORLD, 2 × B_WORLD, and THETA_WORLD.

AGES target selection, objects were classified as compact if they had a CLASS_STAR parameter of ≥ 0.8 in one or more optical bands. This resulted in a small number of emission line galaxies being erroneously classified as compact. For this paper, we classify objects as compact if they have a CLASS_STAR of ≥ 0.7 in two or more of the three optical bands. Of the 288 24 μm sources with AGES spectroscopy which are classified as compact with our CLASS_STAR criterion, 20 are $z < 1$ galaxies which we reclassify as extended objects for the remainder of the paper. Type I quasar candidates are selected from the sample of 24 μm sources with compact optical morphologies (§3). This reduces galaxy contamination while maintaining a high completeness for $z > 1$ quasars. Of the 1182 24 μm sources with $R < 20.2$ extended counterparts and AGES spectroscopy, only two are $z > 1$ type I quasars. We do not attempt to measure the $z < 1$ type I quasar and Seyfert luminosity function, as the host galaxies of $z < 1$ AGNs are sometimes detected and resolved in the deep NDWFS imaging resulting in a complex selection function that depends on host morphology, host luminosity, AGN optical luminosity, redshift and image quality. Our selection criteria also eliminates type II quasars from the sample, which we will discuss in detail in a second paper. Our measurement of the $1 < z < 5$ type I quasar luminosity function and our conclusions are not highly sensitive to our criteria for star-galaxy classification.

2.2. The MIPS Survey

The NDWFS Boötes field was observed simultaneously at 24, 70, and 160 μm with the Multiband Imaging Photometer for *Spitzer* (MIPS; Rieke et al. 2004) as part of the *Spitzer* IRS team's Guaranteed Time Observing programs (Houck et al. 2005). In this paper we only discuss the 24 μm data, as only five of the type I quasars in our sample were detected in the 70 μm and 160 μm imaging. These observations were performed with the "Medium Scan" technique. This observing mode is particularly suitable for high efficiency coverage of wide fields such as Boötes. The 24 μm detector uses a $2\farcs55$ per pixel array of 128×128 elements with a delivered point source full-width at half maximum (FWHM) of $\simeq 6''$. The effective integration time per sky pixel was $\simeq 90$ s. Data reduction was carried out using the MIPS Data Analysis Tool (Gordon et al. 2005). We corrected count rates for dark current, cosmic–rays, and flux non–linearities. These counts were then divided by flat–fields constructed for each position of the scan–mirror which is used in the "Medium Scan" observing mode. The images were corrected for geometric distortions and combined to produce the final 9.93 deg^2 24 μm mosaic. For this work, we selected 24 μm sources from the 8.22 deg^2 of the 24 μm mosaic which overlaps the NDWFS and comprises of two or more individual scans.

As almost all the sources in the MIPS mosaic are unresolved, source extraction and photometry were performed using the stellar PSF fitting technique of the DAOPHOT software (Stetson 1987). An empirical PSF was constructed from the brightest objects found in our mosaic, and it was subsequently fitted to all the sources detected in the map. Allowing for multiple-match fitting to deal with blended cases, we derived the flux density of each source from the scaled fitted PSF and finally applied a slight correction to account for the finite size of the modeled point spread function. Catalog depth was determined by adding artificial point sources to the MIPS mosaic and attempting to recover them with DAOPHOT. We estimate that the 80% completeness limit to be 0.3 mJy.

2.3. The AGN and Galaxy Evolution Survey

The AGN and Galaxy Evolution Survey (AGES, Kochanek et al. in preparation) is obtaining complete spectroscopic samples of galaxies and quasars selected over a broad range of wavelengths in the Boötes field of the NDWFS. The spectra are obtained with Hectospec, a 300-fiber robotic spectrograph on the MMT 6.5-m telescope (Fabricant et al. 1998; Roll, Fabricant, & McLeod 1998). Spectra were extracted and classified using two independent reduction pipelines and then verified by visual inspection. One pipeline is based upon the SDSS spectroscopic data reduction software while the other is a set of customized IRAF scripts. The wavelength coverage of the spectra extends from 3700Å to 9200Å, although some spectra are contaminated redwards of 8500Å by a red leak from an LED in the fiber positioner.

The AGES spectroscopic targets were selected from the April 9, 2004 pre-release versions of the

NDWFS and MIPS 24 μm source catalogs. However, for the remainder of the paper we use the photometry of the third data release of the NDWFS and July 5, 2005 pre-release version of the MIPS 24 μm catalog. These have less artifacts and slightly better photometric calibrations than the earlier catalogs. The spectra are mostly from AGES internal release 1.1 with some additional spectra of R-band selected targets from AGES internal release 2.0. AGES targeted 24 μm sources with fluxes of $S_{24} > 1$ mJy (or $[24] < 16.40$ where [24] is the AB apparent magnitude) which had optically extended $R < 20.2$ counterparts or optically compact $17.2 < R < 21.7$ counterparts. For AGES target selection, objects were classified as compact if their SExtractor CLASS_STAR parameter was ≥ 0.8 in one or more of the B_W, R, or I-bands. To reduce the number of bright ($R \lesssim 18$) galactic stars in the spectroscopic sample, compact sources were not targetted if they had 2MASS counterparts bluer than $J - [24] = -3.51$. The roughly power-law spectra of quasars and the black body spectra of stars make the infrared color differences of these two populations very obvious (e.g., Stern et al. 2005). These criteria led to 1571 spectroscopic targets, and accurate spectroscopic redshifts were obtained for 1449 of them.

2.4. The Multiwavelength Sample

The final, multiwavelength catalog consists of 24 μm sources brighter than 1 mJy with good 24 μm and optical imaging inside the primary AGES target regions. For saturated objects in the NDWFS images, we have used the fourth data release of the Sloan Digital Sky Survey (SDSS DR4; Adelman-McCarthy 2005) for the photometry and classifications. We excluded sources with $R > 17.2$ counterparts within $(20.2 - R)''$ of $R < 15.2$ USNO-A2 stars (Monet et al. 1998) where our ability to detect faint optical counterparts is compromised. We also excised $\gtrsim 1'$ radius regions around Hipparcos stars (Esa 1997), which are occasionally broken up into multiple spurious USNO-A2 catalog entries. This left us with an effective survey area of 7.17 deg^2. Objects with spurious $R > 21.7$ counterparts (e.g., edges of $R \sim 18$ star halos) have been removed from the final catalog. The sky distribution of objects in the catalog is shown in Figure 1.

Table 1 presents the number counts of the 24 μm sources and Figure 2 shows the distribution of their R-band magnitudes. Most of the 24 μm sources are brighter than $R = 22$, and most of these sources are either quasars or $z \lesssim 1$ galaxies. The 17% of 24 μm sources with $R > 21.7$ counterparts include include ultra-luminous infrared galaxies and obscured quasars at $z > 1$ (Houck et al. 2005; Martínez-Sansigre et al. 2005). Type I quasars have relatively bright optical counterparts and mostly compact optical morphologies. AGES spectroscopic redshifts are available for 63% of the $S_{24} > 1$ mJy sources and 92% of the 24 μm sources satisfying the AGES selection criteria.

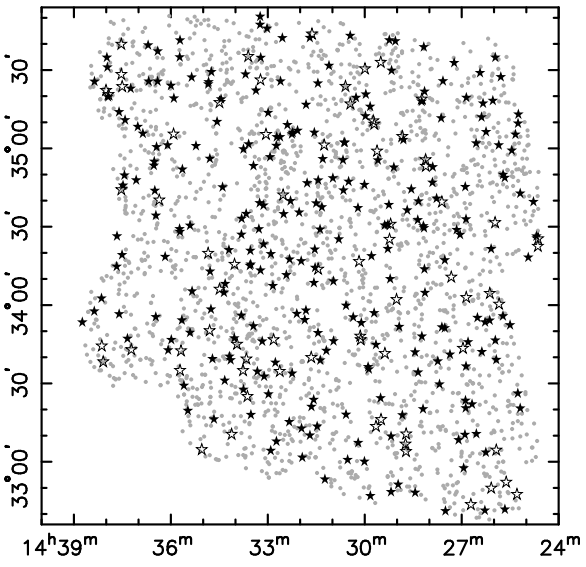

Fig. 1.— The sky distribution of 24 μm sources brighter than 1 mJy in the multiwavelength catalog. Compact objects with and without spectra are shown with solid and open stars respectively. Gray circles denote the locations of sources with extended optical morphologies. The semicircular edges of the sample are an artifact of the circular 1 degree field of view of the Hectospec instrument.

3. THE TYPE I QUASAR SAMPLE

We define our type I quasar sample to be 24 μm sources brighter than 1 mJy with $17.2 < R < 23.5$ compact optical counterparts. The compact optical morphology is due to the observed optical emission being dominated by a relatively unob-

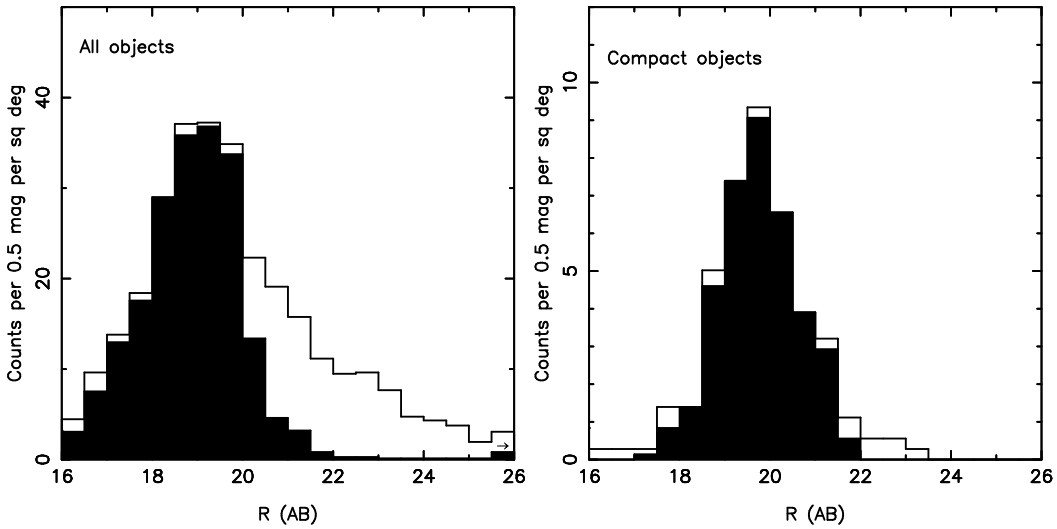

Fig. 2.— The distribution of R-band magnitudes for all (*left*) and optically compact (*right*) 24 μm sources. The distribution of objects with spectroscopic redshifts (from both the literature and AGES) is shown with the shaded histogram. Most (86%) of objects with compact optical morphologies have AGES spectroscopic redshifts.

scured AGN. Our sample is incomplete for $z < 1$ quasars and Seyferts, where AGN host galaxies are sometimes resolved in the NDWFS imaging and AGN host galaxies can contribute significantly to the observed 24 μm flux. The bluest spectroscopic quasar in our sample has a color of $R - [24] = 2.5$ (where $R - [24]$ is the apparent color in AB magnitudes), so we have excluded $R - [24] < 2$ sources from the sample with the expectation that this will not effect the sample completeness for highly luminous quasars. Of the 47 objects excluded with this color criterion, 90% are brighter than $R = 17$ and are almost certainly stars. AGES spectroscopy identified 20 $z < 1$ galaxies which were erroneously classified as compact in the NDWFS, and they were reclassifed as extended and excluded from the quasar sample. Two $R < 20.2$ $z > 1$ quasars which were classified as extended in the optical imaging have been added to the quasar sample. The final sample contains 292 quasars and quasar candidates. Figure 3 shows the redshift distribution of the 270 objects in the sample with AGES spectroscopic redshifts. All the quasars without redshifts are at $z < 3.8$ (or are blends with $z < 3.8$ objects), as they all have B_W detections indicating that the Lyman limit is within or blueward of our B_W filter. The vast majority (83%) of the quasars with spectra and 59% of the candidates without spectra have one or more photons in the XBoötes Chandra imaging survey (Murray et al. 2005). In contrast only 23% of the $z < 1$ galaxies with $S_{24} > 1$ mJy are detected in XBoötes. Quasar candidates without spectra have the same likelihood ($\simeq 10\%$) of having 1.4 GHz counterparts (from de Vries et al. 2002) as spectroscopically confirmed quasars. We therefore expect most of the 22 quasar candidates without spectra to be quasars.

While our R-band spectroscopic flux limit is less sensitive to extinction than standard ultraviolet excess (UVX) searches, it still corresponds to the rest-frame ultraviolet emission of the quasars. As shown in Figure 4, the apparent colors and magnitudes of quasars show some evidence for obscuration since fainter quasars tend to have redder colors that could be explained by modest amounts of extinction. This is consistent with modest dust reddening producing the broad red tail of type I quasar colors (e.g., Richards et al. 2001).

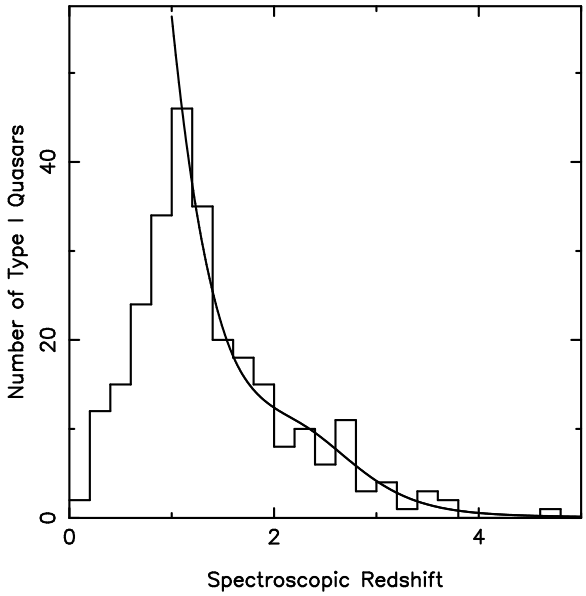

Fig. 3.— The spectroscopic redshift histogram of type I quasars. The sample is incomplete at $z < 1$ as some quasars are classified as extended in the deep NDWFS imaging. The curve is derived from the best-fit luminosity function, and is a good approximation to the $z > 1$ data.

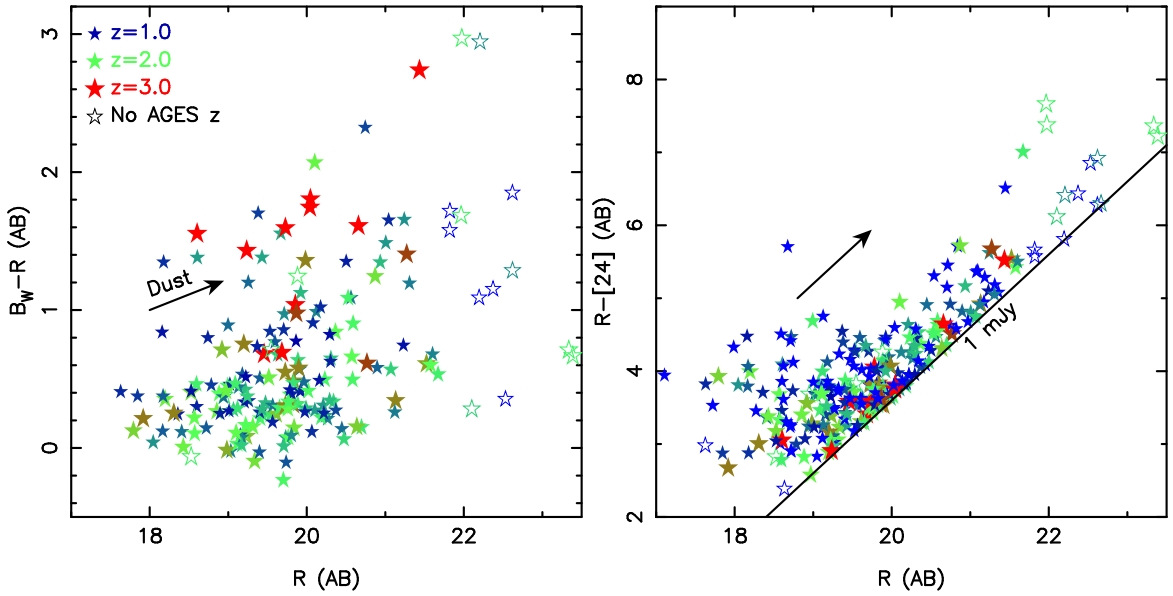

Fig. 4.— The apparent colors of type I quasars. The symbol size and color are a function of redshift. Objects with spectroscopic and photometric redshifts are shown with solid and open symbols respectively. Arrows denote the apparent color vectors for $z = 2$ dust extinction with rest-frame $E(B - V) = 0.1$, using the approximation of Calzetti (1999). Only objects with unsaturated B_W photometry are shown in the left panel. Relatively little dust obscuration can explain much of the dispersion of type I quasar colors.

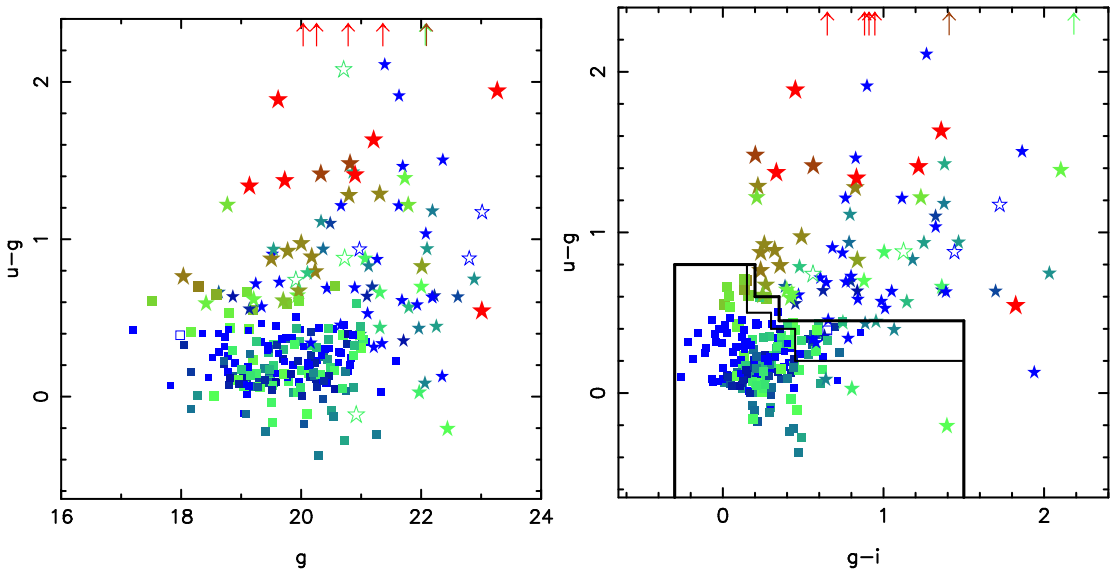

Fig. 5.— SDSS DR4 color-magnitude (left) and color-color (right) diagrams for the 24 μm selected type I quasar sample. As in Figure 4, symbol size and color are a function of redshift, and open symbols denote objects without spectroscopic redshifts. In the right panel, the 2SLAQ selection criteria for $g < 21.15$ and $g < 21.85$ are shown with bold and narrow lines respectively. Quasars selected by the 2SLAQ criteria are shown with squares. Of the 142 $1.0 < z < 2.2$ quasars in the 24 μm sample, 112 (79%) are also selected by the UVX criteria of 2SLAQ.

3.1. Comparison with UVX Surveys

As a check of our sample completeness and to compare our selection criteria with traditional optical surveys, we compared our sample to a sample of UVX quasar candidates. These were selected using the criteria of the 2dF-SDSS Luminous Red Galaxy and Quasar Survey (2SLAQ; Richards et al. 2005) and SDSS DR4 imaging catalogs, which overlap almost all of the Boötes field. The 2SLAQ criteria do not include morphology cuts for most objects, but do include optical color cuts which limit the ability of 2SLAQ to detected reddened and $z > 2.2$ quasars. We restricted the comparison to $R < 19$ quasars because at fainter magnitudes the blue quasars will tend to have $S_{24} < 1$ mJy (see Figure 4). Of the 46 $R < 19$ UVX candidates in Boötes, 38 (83%) are in our 24μm quasar sample. The remaining $R < 19$ UVX candidates are starburst galaxies or $z < 0.3$ quasars whose host galaxies are detected in the NDWFS imaging (and are classified as extended sources). Our 24μm quasar sample is therefore highly complete for type I quasars selected with the UVX technique, particularly at $z > 1$ where quasar hosts are unresolved in the NDWFS imaging.

We now consider the completeness of UVX surveys for quasars selected via their 24 μm flux. Of the 23 $R < 19$ quasars with $1.0 < z < 2.2$ in our 24 μm sample, 19 (83%) are selected by the 2SLAQ UVX criteria. The four $1.0 < z < 2.2$ quasars not selected by the 2SLAQ criteria all have red colors ($u - g > 0.5$ and $R - [24] > 3.7$). Given the problems of small number statistics, this is consistent with the estimate of 90% completeness for the UVX selected quasars from the 2QZ catalog by Smith et al. (2005). However, as shown in Figure 5, the completeness of the UVX samples of quasars above a fixed infrared flux is lower. This is relevant for understanding the accretion history of quasars as the infrared is almost certainly more strongly correlated with the bolometric luminosity than the ultraviolet. If we select the 142 $1.0 < z < 2.2$ quasars brighter than 1 mJy at 24 μm, we find 79% are selected by the 2SLAQ criteria. The quasars not selected by the 2SLAQ criteria are sometimes optically blue and faint, but generally they are red. The me-

dian apparent colors of the 30 $1.0 < z < 2.2$ not selected by the 2SLAQ criteria are $u - g = 0.66$ and $R - [24] = 4.62$. Clearly, there is a significant population of bolometrically luminous red type I quasars which are mostly undetected by traditional UVX quasar surveys. Red type I quasars comprise $\sim 20\%$ of the type I quasar population.

3.2. Morphological Completeness

We can also check the consequences of including only compact sources in our sample. This criterion certainly removes type II quasars from the sample, as their optical emission is dominated by their host galaxies, but it will also remove $z < 1$ type I quasars from our sample when their host galaxies are detected in the deep NDWFS images. Thus, when we evaluate the quasar luminosity function in §4, we restrict the analysis to $z > 1$ quasars. AGES targeted both compact and extended $17.2 < R < 20.2$ sources, so for this magnitude range we can estimate the incompleteness due to compact selection criteria. Of 130 24μm sources with $z > 1$ and $R < 20.2$, only two quasars (1.5%) were classified as extended sources. These objects have been added to our spectroscopic quasar sample. One is close to a foreground star while the other is a blend with a galaxy, which may or may not be physically associated with the quasar. At $20.2 < R < 21.7$, we assume the $z > 1$ quasar sample is 1.5% incomplete due to quasars being classified as extended in the optical imaging. Thus, the morphology cut should only affect the sample completeness at levels well below our statistical uncertainties.

3.3. Spectroscopic Completeness

We can see in Figures 2 and 4 that the vast majority of $S_{24} > 1$ mJy type I quasars are brighter than our spectroscopic limit of $R = 21.7$ and have spectroscopic redshifts. The number of $S_{24} > 1$ mJy type I quasars is clearly decreasing with increasing magnitude at $R > 21.7$. Unlike UVX criteria, our selection criteria do not intrude into the main locus of type I quasar colors. We can use a relatively simple model of the spectroscopic completeness, and our estimate of the luminosity function is not particularly sensitive to changes in this model.

To model the spectroscopic completeness, we assume the distribution of rest-frame $R - [24]$ colors for $z > 1$ type I quasars is neither a function of luminosity or redshift. We measure this distribution using the observed colors of $z > 1$ quasars and k-corrections derived from the higher mid-infrared (MIR) flux quasar spectral energy distribution (SED) of Hatziminaoglou et al. (2005). When spectroscopic redshifts are unavailable, we estimate photometric redshifts by searching for the nearest neighbor in color-space with a spectroscopic redshift. As shown in Figure 6, the apparent $R-[24]$ colors of quasars are a weak function of redshift so relatively inaccurate photometric redshifts can be used to determine rest-frame colors (but not luminosities).

Type I quasars fainter than $R = 23.5$ are not included in our sample, as they are not classified as compact sources. We include a completeness correction for these objects by assuming their color distrbution is identical to quasars with higher 24 μm fluxes and that the shape of their 24 μm number count distribution is identical to that of bluer quasars. We estimate there are four $z > 1$ type I quasars fainter than $R = 23.5$, and include this in our completeness estimates though this has little effect on our measured luminosity function.

Our estimate of the rest-frame $R-[24]$ distribution for $z > 1$ quasars is shown in the left panel of Figure 7. To derive the distribution of apparent R-band magnitudes as a function of both 24 μm flux and redshift, we used this model and applied the k-corrections derived from the higher MIR quasar SED of Hatziminaoglou et al. (2005). We multiplied the distribution of R-band magnitudes by the measured completeness of as a function of R-band magnitude to determine the spectroscopic completeness of the sample as a function of 24 μm flux and redshift. As shown in the right panel of Figure 7, the spectroscopic completeness peaks at a 24 μm flux of $\sim$ 7mJy, which corresponds to $17.2 < R < 20.2$ where the AGES spectroscopic completeness plateaus at $\simeq 95\%$. The spectroscopic completeness then declines to $\sim 80\%$ at both 1 mJy (because of the unmeasured redshifts) and at 15 mJy (because of the AGES $R > 17.2$ criterion).

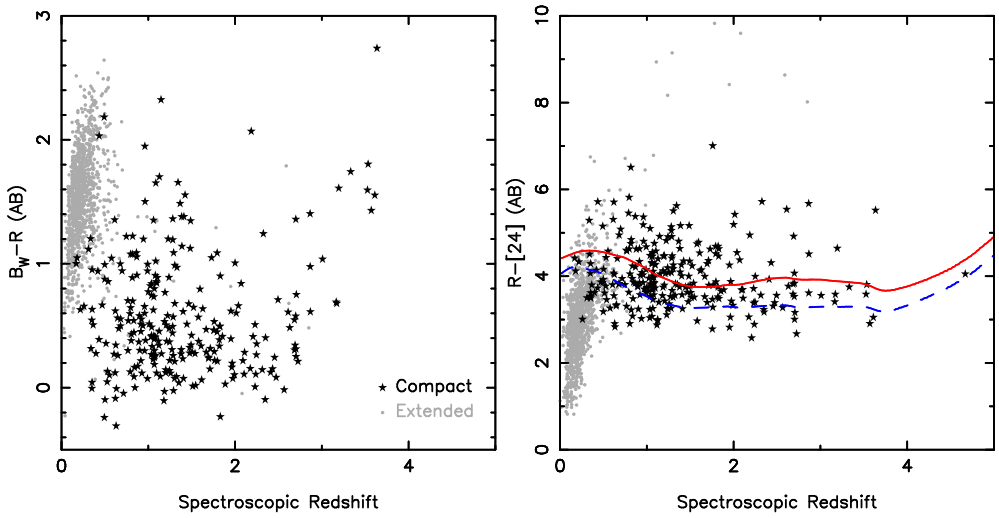

Fig. 6.— The apparent colors of 24 μm sources in the Boötes field as a function of spectroscopic redshift. Optically compact objects are shown with stars while extended objects are shown with dots. Two quasar templates from Hatziminaoglou et al. (2005) are also shown. The dashed line denotes the template derived from 35 SDSS quasars in the SWIRE ELAIS-N1 field while the solid line denotes the higher MIR flux quasar template, which is a better fit to the median color of our sample. The apparent $R-[24]$ color of type I quasars is a weak function of redshift in the range $1 < z < 5$. The spectroscopic sample contains very red and bolometrically luminous quasars, though at the limits of the 24 μm and AGES spectroscopic samples we are restricted to $R-[24] < 5.3$ objects.

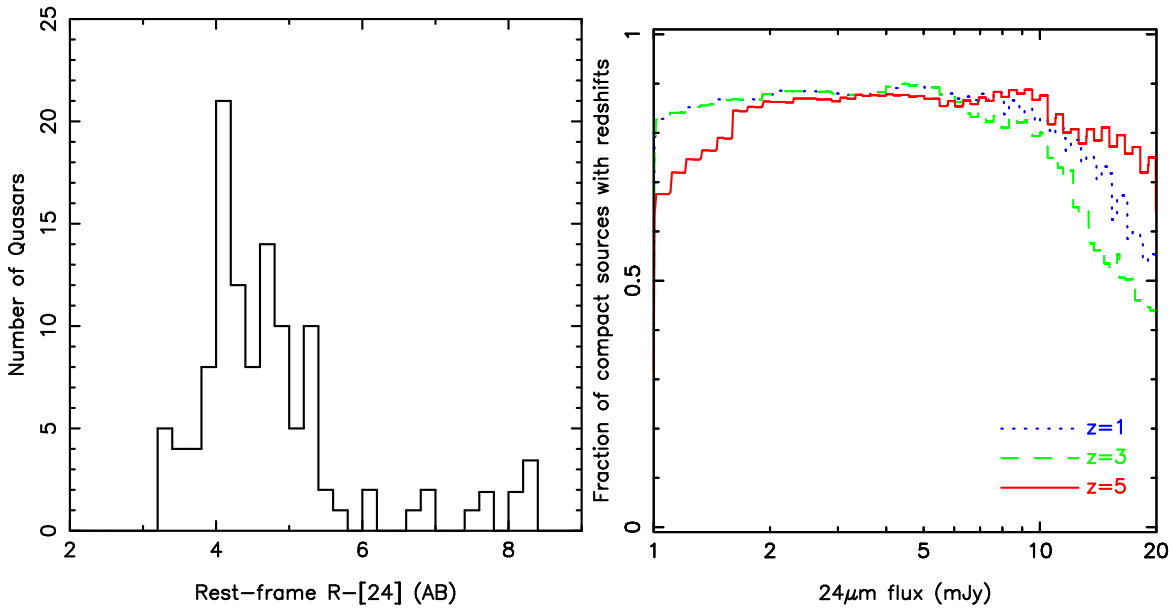

Fig. 7.— The distribution of rest-frame colors (left panel) and the estimated spectroscopic completeness (right panel) for the 24 μm selected type I quasar sample. For the redshift range $1 < z < 4$, all $S_{24} > 1$ mJy type I quasars with restframe $R-[24] < 6$ are brighter than our $R = 21.7$ spectroscopic limit. The plateau of the spectroscopic completeness corresponds to $17.2 < R < 20.2$, where the AGES spectroscopic completeness for optically compact sources is $\simeq 95\%$.

4. LUMINOSITY FUNCTION OF TYPE I QUASARS

The luminosity function of quasars is one of the principal constraints on the accretion history of the most massive blackholes (e.g., Kauffmann & Haehnelt 2000). At the highest luminosities the fraction of type II quasars is thought to be low (e.g., Ueda et al. 2003; Hao et al. 2005), although current studies do not include radio-quiet quasars obscured in both the optical and X-ray. If there are few type II quasars at very high luminosities then the type I quasar luminosity function provides a good approximation of the overall quasar space density at the highest luminosities.

We evaluate the luminosity function using 183 $z > 1$ quasars with spectroscopic redshifts. As discussed earlier, the deep NDWFS images can sometimes detect the host galaxy of $z < 1$ quasars so modeling the completeness would require a detailed treatment of star/galaxy classification as a function of quasar luminosity, host luminosity, host morphology and image quality. Several $z < 1$ extended objects are classified as broadline AGNs by the AGES pipeline and are not included in our sample of 292 type I quasars. The present sample does not include $z > 5$ quasars because of the bright R-band magnitude limit. In the 2005 AGES sample, which uses a fainter I-band selection criterion, appreciable numbers of $z > 5$ quasars are found, but they are fainter than $S_{24} = 1$ mJy.

We estimated the rest-frame 8 μm absolute magnitudes of the sample using the AGES spectroscopic redshifts, the 24 μm flux, and the higher MIR flux quasar SED of Hatziminaoglou et al. (2005). For the redshift range $1 < z < 5$, observed 24 μm corresponds to rest-frame 12 μm to 4 μm, so our 8 μm absolute magnitudes are not very sensitive to our choice of quasar SED. Using a bluer quasar SED template, derived from 35 SDSS quasars in the SWIRE ELAIS-N1 field (Hatziminaoglou et al. 2005), alters the absolute magnitudes of individual quasars by only a few tenths of a magnitude, our luminosity function parameters by $\lesssim 1\sigma$, and our conclusions little. The distribution of absolute magnitudes as a function of redshift is shown in Figure 8. Most objects have 8 μm absolute magnitudes brighter than -25, which corresponds to 1.6×10^{44}ergs s^{-1} in νF_ν.

We estimate the luminosity function using the maximum likelihood method of Marshall et al. (1983). We assume the luminosity function is a power-law of the form

$$\phi_8(L, z)dL \propto \left(\frac{L}{L^*(z)}\right)^{\alpha} dL \qquad (1)$$

where α is a constant and $L^*(z)$ describes the pure luminosity evolution of the quasar luminosity function. This can also be written as a function of absolute magnitude;

$$\phi_8(M, z)dM \propto 10^{0.4(\alpha+1)[M^*(z)-M]}dM. \qquad (2)$$

Optical surveys generally require models where the slope of the luminosity function becomes shallower for low luminosity quasars (e.g., Schmidt & Green 1983; Boyle, Shanks, & Peterson 1988; Croom et al. 2004; Wolf et al. 2003b; Richards

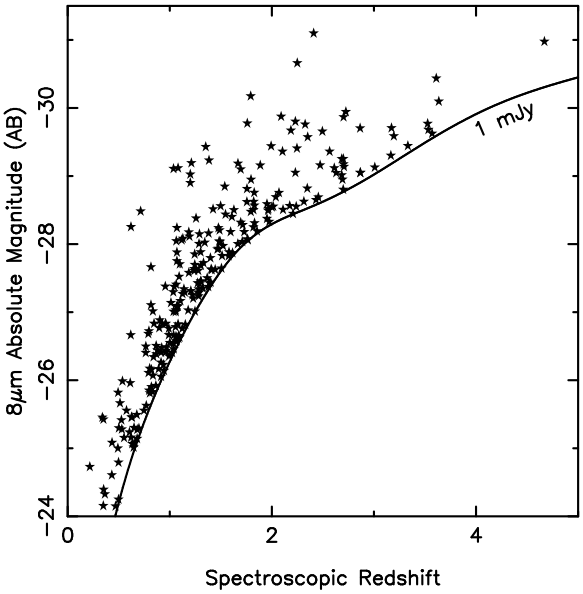

Fig. 8.— The distribution of the 8 μm absolute magnitudes of the type I quasar sample as a function of spectroscopic redshift. Absolute magnitudes were determined using the measured 24 μm fluxes, spectroscopic redshifts, and the higher MIR flux template of Hatziminaoglou et al. (2005). Since rest-frame 8 μm roughly corresponds to observed 24 μm, we have measured 8 μm absolute magnitudes and the 8 μm luminosity function. The $M_B < -22.3$ criterion for quasars (Véron-Cetty & Véron 2003) roughly corresponds to an 8 μm AB absolute magnitude limit of -25.3.

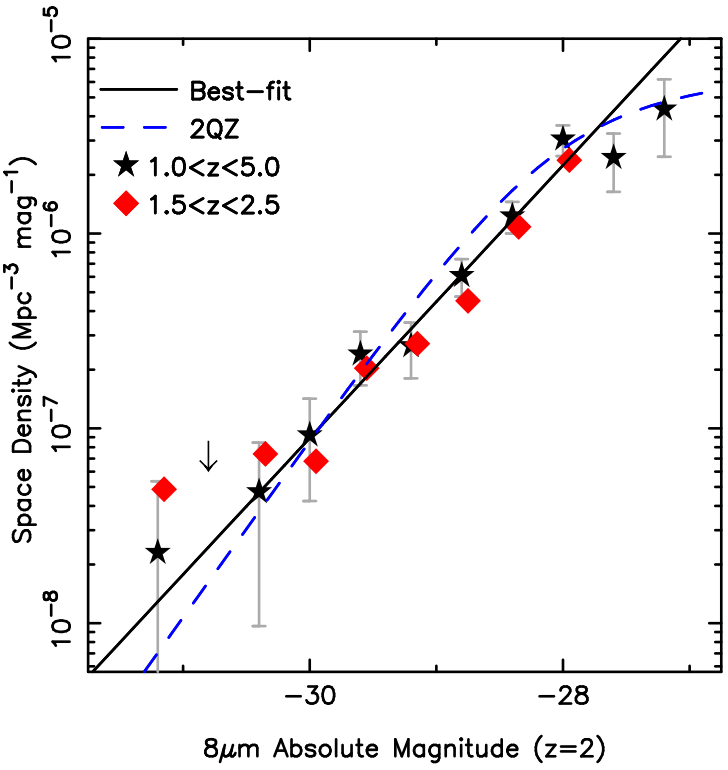

Fig. 9.— The 8 μm luminosity function of $z = 2$ type I quasars. The solid line is the best-fit power-law while the datapoints are determined using $1/V_{max}$ with quasar luminosities adjusted for evolution. For clarity, we only show error bars and 3σ upper limits for the $1/V_{max}$ luminosity function determined with $1 < z < 5$ quasars. For comparison, the dashed line shows the 2QZ luminosity function (Croom et al. 2004) where we have assumed that $B_J - [8] = 3.08$ (AB) for blue quasars. An AB absolute magnitude of -28.5 corresponds to 4.11×10^{45}ergs s^{-1} in νF_ν.

et al. 2005), but a single power-law fits our data reasonably well. When we tried fitting a double power-law to the data, we were unable to precisely constrain the faint-end slope due to the limited size and luminosity range of our sample. We modeled the evolution of the quasar luminosity function using pure luminosity evolution where

$$L^*(z) = L^*(0)10^{k_1 z + k_2 z^2 + k_3 z^3} \quad (3)$$

with k_1, k_2, and k_3 being constants. This is similar to the polynomial used by optical quasar surveys such as the 2QZ, and aids comparisons with the previous surveys. Unlike optical quasar samples, we have no difficulty finding quasars at $2.3 < z < 3.0$ (where the optical colors match those of main sequence stars), so we can track the evolution of the luminosity function through its peak. This forces us to add the $k_3 z^3$ term to the polynomial so that the evolution on the high redshift side of the peak is not forced to be identical to that on the low redshift side of the peak by the symmetry of the equation. This pure luminosity evolution model is sufficient for a sample of $\sim 10^2$ quasars – larger samples containing $\sim 10^4$ quasars require more complex models (e.g., Croom et al. 2004).

In Figure 9 we plot our best-fit luminosity function for $z = 2$ type I quasars and our best-fit parameters are summarized in Table 2. Only the 183 quasars with spectroscopic redshifts of $z > 1$ were used to measure the luminosity function. We used the completeness estimates described in §3.2 and §3.3 to correct for the spectroscopic and morphological incompleteness of the sample. We also generated an estimate of the $z = 2$ luminosity function using the $1/V_{max}$ method after attempting to remove the effects of evolution. For each quasar,

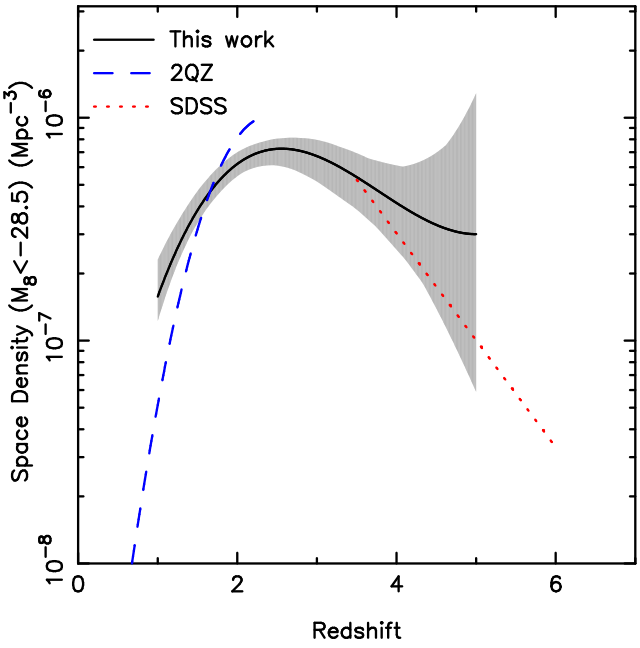

Fig. 10.— The space density of type I quasars brighter than $M = -28.5$ (4.11×10^{45} ergs s^{-1}) at 8 μm. The shaded region denotes the area bounded by the $\pm 1\sigma$ uncertainties. We have overplotted space densities from the 2QZ (Croom et al. 2004) and SDSS (Fan et al. 2004) by assuming that the Hatziminaoglou et al. (2005) template derived from 35 SDSS quasars approximates the median color for these samples. This is only an approximation since it ignores the spectral diversity of blue quasars. The space density of bright quasars rapidly evolves and peaks at $z = 2.5 \pm 0.3$.

we estimated a $z = 2$ absolute magnitude by assuming

$$M(2) = M(z) + 2.5(k_1 z + k_2 z^2 + k_3 z^3) - 2.5(2k_1 + 4k_2 + 8k_3) \quad (4)$$

with our best-values of k_1, k_2, and k_3 (Table 2). This allows us to use quasars from a broad range of redshifts to estimate a $1/V_{max}$ luminosity function. We have used a statistical representation of the evolution rather than a model for the evolution of individual quasars. A large number of black holes undergoing relatively brief episodes of quasar activity can produce a luminosity function that mimics a smaller population of quasars undergoing luminosity evolution (e.g., Kauffmann & Haehnelt 2000). Our measurements of the $z = 2$ quasar luminosity function using the $1/V_{max}$ method are plotted in Figure 9 and tabulated in Table 3. Our best fit power-law and $1/V_{max}$ luminosity functions agree well. The very faintest quasars show a slight departure from the power-law, but we cannot detect it with any precision when we include a break in our maximum likelihood models. Figure 3 shows that the observed and model distribution of the $1 < z < 5$ quasars in redshift agree well, though our results cannot be naively extrapolated to other redshifts.

Our best-fit parameters for the quasar luminosity function are summarized in Table 2 along with the luminosity function parameters for the 2QZ (Croom et al. 2004) for comparison. Our luminosity function is not as steep as the bright-end of the 2QZ luminosity function. However, we are measuring quasars that are slightly brighter than the break in the 2QZ luminosity function, where the power-law index changes from -3.3 to $\simeq -1.5$. As shown in Figure 9, the $z = 2$ luminosity functions of this work and the 2QZ are similar for quasars within our luminosity range. Figure 10 plots the measured evolution of the quasar space density from our 24 μm quasar sample and the optically selected 2QZ and SDSS samples. The three surveys indicate a peak in quasar activity occurs at $z \simeq 2.5$.

If the dust obscuration of AGNs is a function of bolometric luminosity (e.g., Hao et al. 2005), then the shape of the quasar luminosity function should vary with color. For example, if obscuration increases with decreasing luminosity, then the luminosity function of reddened quasars should be steeper than that of blue quasars. We divided our sample into quasars with $R-[24]$ colors that are redder and bluer than the higher MIR flux quasar template of Hatziminaoglou et al. (2005). This rest-frame color cut of $R-[24]=4.4$ corresponds to an apparent color cut of $R-[24]\sim 3.8$ over the redshift range $1<z<4$. As the spectroscopic subsamples contain $\simeq 90$ quasars each, the uncertainties for α are prohibitively large if we let evolution parameters (k_1, k_2, and k_3) float. We have therefore fixed the values of the evolution parameters to the fit derived with the entire quasar sample.

Our best fit luminosity function parameters are given in Table 2. The power-law indices (α) of the blue and red subsamples differ by only 1σ. This is not completely unexpected as the range of dust obscuration probed by our samples is limited. As shown in Figure 4, at $z=2$ our $17.2<R<21.7$ spectroscopic sample spans a range of $E(B-V)$ values of ~ 0.4. In contrast, the range of $E(B-V)$ values spanned by Seyfert Is and IIs is ~ 100 (e.g., Clavel et al. 2000). At present, the dependence of the dust obscuration on bolometric luminosity has only been seen in comparisons of type I and II AGNs (Hao et al. 2005), so a complete sample of type II quasars may be required to understand the relationship between dust obscuration and luminosity for the most bolometrically luminous quasars.

5. TYPE II QUASARS

Ideally we would measure the luminosity functions of both type I and II quasars. However, spectroscopic redshifts for $z>1$ type II quasars are non-trivial as their optical counterparts can be extremely faint (e.g., Houck et al. 2005; Martínez-Sansigre et al. 2005). Photometric redshifts are also difficult as the broad-band SED includes unknown contributions from the AGN, host galaxy, and dust (Zakamska et al. 2005). In this section, we provide a brief discussion of the type II quasar candidates. A spectroscopic campaign to measure the redshifts of the most luminous type II quasar candidates is ongoing, and a future paper will discuss the luminosity function of these objects in detail.

We designate all 24 μm sources brighter than 1 mJy with extended $R>21.7$ optical counterparts (or counterparts too faint for reliable morphological classification) as $z>1$ type II quasar candidates. At $z\sim 1$, $R=21.7$ corresponds to a blue $\simeq L^*$ galaxy (Wolf et al. 2003a). Unlike radio and X-ray surveys, we can detect $z>1$ type II quasars which are both radio-quiet and Compton thick. The main contaminants of the sample will be starburst galaxies, $z<1$ type II AGNs, and reddened type I quasars. There are 376 $z>1$ type II quasar candidates in our survey area. Only 20 of these objects have spectroscopic redshifts, mostly from Houck et al. (2005), and all but one of these redshifts are in the range $0.7<z<3.0$.

The optical colors of the type II quasars candidates are shown in Figure 11. The locus of blue B_W-R and red $R-I$ colors are consistent with $1<z<3$ host galaxies. Type II candidates with counterparts in the radio catalog of de Vries et al. (2002) and the XBoötes Chandra imaging survey (Murray et al. 2005) are also shown in Figure 11. As the 0.5 to 7 keV background of the XBoötes survey is only $\simeq 0.03$ counts within a $2''$ radius aperture, the detection of a single X-ray photon within this aperture is significant in the vast majority of cases, and at $z=1$ a single photon in XBoötes corresponds to an X-ray luminosity of $\sim 10^{43}$ ergs s^{-1}. For a $z>1$ source this is a strong indicator of AGN activity, as the implied luminosity is an order of magnitude more than low redshift starbursts including Arp 220, which has an observed X-ray luminosity of 1.4×10^{41} ergs s^{-1} (McDowell et al. 2003). One-third of the type II quasar candidates have one or more X-ray photons in the Chandra images, and this increases to 45% for candidates brighter than 2 mJy.

We have determined upper limits for the fraction of $z>1$ obscured quasars as a function of flux by dividing the number of $z>1$ type II candidates by the total number of $z>1$ type I and type II candidates. Contamination of our $z>1$ type I sample is low and contamination of the $z>1$ type II candidate sample by $z<1$ AGNs and starbursts could be high, so this fraction is an upper limit. Upper limits for the fraction of ob-

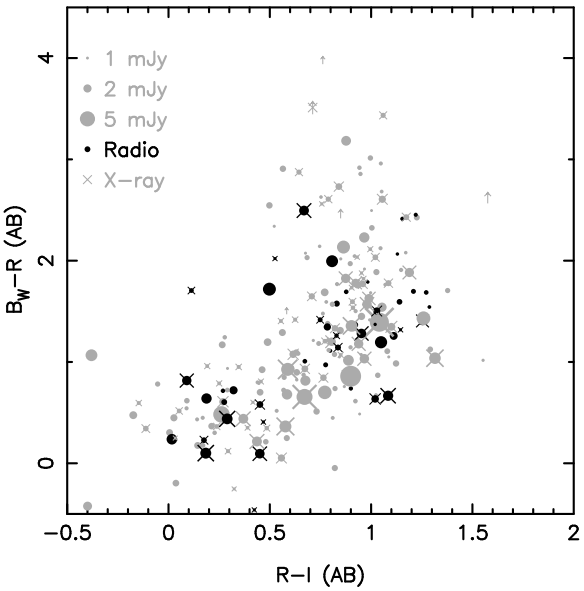

Fig. 11.— The $B_W RI$ colors of $R > 21.7$ type II quasar candidates. Symbol size is a function of 24 μm flux and objects with radio (bold symbols) and X-ray counterparts (crosses) are highlighted. The optical colors of most objects are consistent with $1 < z < 3$ host galaxies. Candidates with X-ray counterparts are almost certainly AGNs, and they comprise 32% and 45% of the candidates brighter than 1 mJy and 2 mJy respectively.

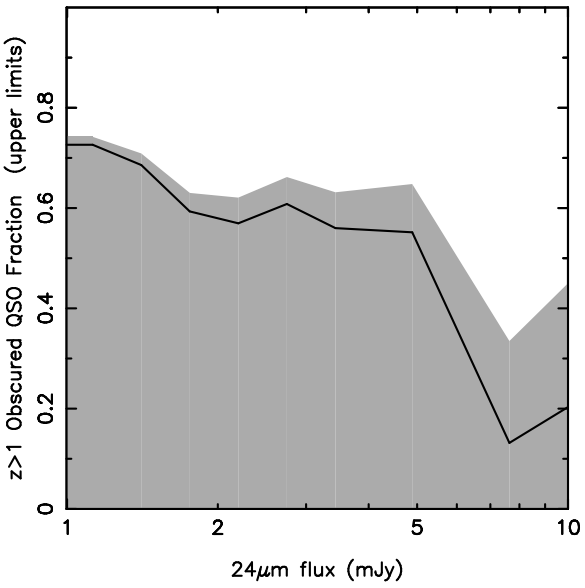

Fig. 12.— Upper limits on the fraction of obscured quasars as a function of observed 24μm flux. The shaded area denotes the region below our best estimate of the obscured fraction plus the 1σ statistical uncertainties. Our sample of type II quasar candidates could be contaminated by starburst galaxies, so we can only set upper limits in the absence of spectroscopic confirmation. The fraction of obscured quasars could be as high as 70% at 1 mJy, and then decreases with increasing 24 μm flux.

scured quasars as a function of 24 μm flux are plotted Figure 12. This should not be confused with the fraction of obscured quasars as a function of bolometric luminosity, which would require accurate redshift information. We do not know if the obscured quasars have systematically lower redshifts (and bolometric luminosities) than the type I quasars with comparable 24 μm fluxes. We also do not know the extent of dust absorption of rest-frame ~ 8 μm emission in these AGNs. Despite these caveats, it is reasonable to conclude that the ratio of obscured and unobscured AGNs near the break in optical luminosity function (roughly $S_{24} = 1$ mJy) is of order unity. This is consistent with studies of X-ray selected AGNs, optically selected Seyferts, and small samples of infrared selected $z > 1$ type II quasars (e.g., Steffen et al. 2003; Ueda et al. 2003; Hao et al. 2005; Martínez-Sansigre et al. 2005). The fraction of obscured quasars decreases with increasing flux, which is similar to the trend observed as a function of luminosity in X-ray and optical samples (e.g., Ueda et al. 2003; Hao et al. 2005). If the obscured fraction is decreasing rapidly with increasing luminosity, the type I quasar luminosity function approximates the luminosity function of all quasars at the highest luminosities. However, to confirm this will require complete spectroscopic samples of type II quasars.

6. SUMMARY

We have measured the 8 μm luminosity function of type I quasars as a function of redshift using 292 quasars and quasar candidates selected from *Spitzer Space Telescope* 24 μm imaging of the NDWFS Boötes field. Spectroscopic redshifts for 270 of these quasars were measured as part of the AGES survey of Boötes. We were able to de-

tect reddened type I quasars which were missed by UVX quasar surveys, and these comprise approximately a fifth of the type I quasar population. The type I quasar luminosity function at 8 μm, and its evolution with redshift, is very similar to quasar luminosity functions at optical and ultraviolet wavelengths. Figure 10 illustrates the evolution of the space density of type I quasars. There is qualitative agreement between our best-fit luminosity function and the 2QZ and SDSS, despite our sample being selected at 24 μm rather than the optical. We directly detect the peak in quasar activity at $z = 2.6 \pm 0.3$, which has been difficult to directly measure with optical quasar surveys because it corresponds to the redshift range where quasar optical colors are similar to those of stars.

Our best-fit model indicates that the quasar space density declines by a factor of $\simeq 2$ between $z = 2.5$ and $z = 4.0$, though this decline has low significance. If we fit our data with a model where the space density is constant after z_{peak} then our luminosity function parameters change by $\lesssim 1\sigma$. However, such a model disagrees with the results of optical surveys of $z > 3$ quasars (Schmidt, Schneider, & Gunn 1995; Fan et al. 2004). Thus, unless the obscured quasar fraction increases at high redshift, our study and previous optical quasar surveys indicate that the quasar space density declines at $z > 3$.

While the evolution of the type I quasar space density has been measured over a broad range of wavelengths, the evolution of type II quasars remains uncertain. Figure 12 indicates that they could comprise 70% of $z > 1$ quasars brighter than 1 mJy, though this fraction decreases with increasing flux and luminosity. Until there is a systematic campaign to measure the spectroscopic redshifts of type II quasars, the 8 μm luminosity function of all quasars will remain uncertain.

We thank our colleagues on the NDWFS, MIPS, IRS, and AGES teams. This paper would not have been possible without the efforts of the KPNO and MMT observing support staff. We are grateful to Frank Valdes, Lindsey Davis and the IRAF team for the packages used to reduce the imaging data. We thank Alyson Ford, Lissa Miller, and Jennifer Claver, for reducing much of the KPNO MOSAIC data used for this paper. Evanthia Hatziminaoglou kindly provided the quasar SED templates prior to publication. Gordon Richards provided many useful suggestions with regards to the survey technique and manuscript. This work is based in part on observations made with the *Spitzer Space Telescope*, which is operated by the Jet Propulsion Laboratory, California Institute of Technology under NASA contract 1407. This research was supported by the National Optical Astronomy Observatory which is operated by the Association of Universities for Research in Astronomy (AURA), Inc. under a cooperative agreement with the National Science Foundation. Spectroscopic observations reported here were obtained at the MMT Observatory, a joint facility of the Smithsonian Institution and the University of Arizona.

REFERENCES

Adelman-McCarthy, J. K. 2005, ArXiv Astrophysics e-prints

Antonucci, R. 1993, ARA&A, 31, 473

Bertin, E., & Arnouts, S. 1996, A&AS, 117, 393

Boyle, B. J., Shanks, T., & Peterson, B. A. 1988, MNRAS, 235, 935

Calzetti, D. 1999, Ap&SS, 266, 243

Clavel, J., Schulz, B., Altieri, B., Barr, P., Claes, P., Heras, A., Leech, K., Metcalfe, L., et al. 2000, A&A, 357, 839

Croom, S. M., Smith, R. J., Boyle, B. J., Shanks, T., Miller, L., Outram, P. J., & Loaring, N. S. 2004, MNRAS, 349, 1397

de Vries, W. H., Morganti, R., Röttgering, H. J. A., Vermeulen, R., van Breugel, W., Rengelink, R., & Jarvis, M. J. 2002, AJ, 123, 1784

Dunlop, J. S., & Peacock, J. A. 1990, MNRAS, 247, 19

Esa, . 1997, VizieR Online Data Catalog, 1239, 0

Fabricant, D. G., Hertz, E. N., Szentgyorgyi, A. H., Fata, R. G., Roll, J. B., & Zajac, J. M. 1998, in Proc. SPIE Vol. 3355, p. 285-296, Optical Astronomical Instrumentation, Sandro D'Odorico; Ed., 285–296

Fan, X., Hennawi, J. F., Richards, G. T., Strauss, M. A., Schneider, D. P., Donley, J. L., Young, J. E., Annis, J., et al. 2004, AJ, 128, 515

Gordon, K. D., Rieke, G. H., Engelbracht, C. W., Muzerolle, J., Stansberry, J. A., Misselt, K. A., Morrison, J. E., Cadien, J., et al. 2005, PASP, 117, 503

Hao, L., Strauss, M. A., Fan, X., Tremonti, C. A., Schlegel, D. J., Heckman, T. M., Kauffmann, G., Blanton, M. R., et al. 2005, AJ, 129, 1795

Hatziminaoglou, E., Pérez-Fournon, I., Polletta, M., Afonso-Luis, A., Hernán-Caballero, A., Montenegro-Montes, F. M., Lonsdale, C., Xu, C. K., et al. 2005, AJ, 129, 1198

Hopkins, P. F., Hernquist, L., Cox, T. J., Di Matteo, T., Robertson, B., & Springel, V. 2005, ApJ, 630, 716

Houck, J. R., Soifer, B. T., Weedman, D., Higdon, S. J. U., Higdon, J. L., Herter, T., Brown, M. J. I., Dey, A., et al. 2005, ApJ, 622, L105

Jannuzi, B. T., & Dey, A. 1999, in Astronomical Society of the Pacific Conference Series, ed. A. J. Bunker & W. J. M. van Breugel, 111

Kauffmann, G., & Haehnelt, M. 2000, MNRAS, 311, 576

Kron, R. G. 1980, ApJS, 43, 305

Lawrence, A. 1991, MNRAS, 252, 586

Marshall, H. L., Tananbaum, H., Avni, Y., & Zamorani, G. 1983, ApJ, 269, 35

Martínez-Sansigre, A., Rawlings, S., Lacy, M., Fadda, D., Marleau, F. R., Simpson, C., Willott, C. J., & Jarvis, M. J. 2005, Nature, 436, 666

McDowell, J. C., Clements, D. L., Lamb, S. A., Shaked, S., Hearn, N. C., Colina, L., Mundell, C., Borne, K., et al. 2003, ApJ, 591, 154

Monet, D. B. A., Canzian, B., Dahn, C., Guetter, H., Harris, H., Henden, A., Levine, S., Luginbuhl, C., et al. 1998, VizieR Online Data Catalog, 1252, 0

Murray, S. S., Kenter, A., Forman, W. R., Jones, C., Green, P. J., Kochanek, C. S., Vikhlinin, A., Fabricant, D., et al. 2005, ArXiv Astrophysics e-prints

Richards, G. T., Croom, S. M., Anderson, S. F., Bland-Hawthorn, J., Boyle, B. J., De Propris, R., Drinkwater, M. J., Fan, X., et al. 2005, MNRAS, 360, 839

Richards, G. T., Fan, X., Schneider, D. P., Vanden Berk, D. E., Strauss, M. A., York, D. G., Anderson, J. E., Anderson, S. F., et al. 2001, AJ, 121, 2308

Rieke, G. H., Young, E. T., Engelbracht, C. W., Kelly, D. M., Low, F. J., Haller, E. E., Beeman, J. W., Gordon, K. D., et al. 2004, ApJS, 154, 25

Roll, J. B., Fabricant, D. G., & McLeod, B. A. 1998, in Proc. SPIE Vol. 3355, p. 324-332, Optical Astronomical Instrumentation, Sandro D'Odorico; Ed., 324–332

Schmidt, M., & Green, R. F. 1983, ApJ, 269, 352

Schmidt, M., Schneider, D. P., & Gunn, J. E. 1995, AJ, 110, 68

Smith, R. J., Croom, S. M., Boyle, B. J., Shanks, T., Miller, L., & Loaring, N. S. 2005, MNRAS, 359, 57

Steffen, A. T., Barger, A. J., Cowie, L. L., Mushotzky, R. F., & Yang, Y. 2003, ApJ, 596, L23

Stern, D., Eisenhardt, P., Gorjian, V., Kochanek, C. S., Caldwell, N., Eisenstein, D., Brodwin, M., Brown, M. J. I., et al. 2005, ApJ, 631, 163

Stetson, P. B. 1987, PASP, 99, 191

Ueda, Y., Akiyama, M., Ohta, K., & Miyaji, T. 2003, ApJ, 598, 886

Véron-Cetty, M.-P., & Véron, P. 2003, A&A, 412, 399

Wolf, C., Meisenheimer, K., Rix, H.-W., Borch, A., Dye, S., & Kleinheinrich, M. 2003a, A&A, 401, 73

Wolf, C., Wisotzki, L., Borch, A., Dye, S., Kleinheinrich, M., & Meisenheimer, K. 2003b, A&A, 408, 499

Zakamska, N. L., Schmidt, G. D., Smith, P. S., Strauss, M. A., Krolik, J. H., Hall, P. B., Richards, G. T., Schneider, D. P., et al. 2005, AJ, 129, 1212

This 2-column preprint was prepared with the AAS LaTeX macros v5.2.

Table 1

Compact and extended object number counts for the multiwavelength sample.

24 μm flux (mJy)	Total	AGES Spectra	Number counts $R \leq 17.2$	$17.2 < R \leq 20.2$	$20.2 < R \leq 21.7$	$21.7 < R \leq 23$	$R > 23.0$[a]
Optically compact sources[b]							
1 - 50	337	268	45	197	81	12	2
1 - 2	222	181	23	120	67	10	2
2 - 3	54	46	5	40	9	0	0
3 - 4	21	16	5	13	3	0	0
4 - 5	7	6	1	5	1	0	0
5 - 6	8	3	2	4	1	1	0
6 - 7	6	4	1	4	0	1	0
7 - 8	4	4	0	4	0	0	0
8 - 9	3	2	1	2	0	0	0
9 - 10	0	0	0	0	0	0	0
10 - 20	9	5	5	4	0	0	0
20 - 30	2	1	1	1	0	0	0
30 - 40	1	0	1	0	0	0	0
40 - 50	0	0	0	0	0	0	0
Optically extended sources							
1 - 50	1965	1181	232	1061	296	170	206
1 - 2	1322	735	86	700	229	138	169
2 - 3	324	224	41	201	37	17	28
3 - 4	128	87	27	74	12	11	4
4 - 5	65	43	17	33	10	0	5
5 - 6	33	27	10	18	3	2	0
6 - 7	20	13	7	9	4	0	0
7 - 8	15	14	6	9	0	0	0
8 - 9	9	6	4	3	1	1	0
9 - 10	8	6	3	5	0	0	0
10 - 20	24	15	15	8	0	1	0
20 - 30	12	7	12	0	0	0	0
30 - 40	3	2	3	0	0	0	0
40 - 50	2	2	1	1	0	0	0

[a]At faint magnitudes, where the SExtractor star-galaxy classifier is unreliable, we assume optical counterparts are extended.

[b]$z < 1$ galaxies with AGES spectra that were classified as compact in the NDWFS imaging have been reclassified as extended objects.

Table 2

Luminosity Function Parameters

Parameter	All	$R - [24] > 4.4$[a]	$R - [24] < 4.4$[a]	2QZ[b]
$\phi_8(-26,0)[10^{-7}\mathrm{Mpc}^{-3}\mathrm{mag}^{-1}]$	$4.84\pm^{5.15}_{3.37}$	2.35 ± 0.28	2.44 ± 0.26	-
$\phi_8(-29,2)[10^{-7}\mathrm{Mpc}^{-3}\mathrm{mag}^{-1}]$	4.46 ± 0.53	2.16 ± 0.26	2.26 ± 0.25	-
α	$-2.75\pm^{0.17}_{0.11}$	-2.82 ± 0.14	-2.66 ± 0.13	-3.31
k_1	$+1.15 \pm 0.34$	$+1.15$	$+1.15$	$+1.39$
k_2	-0.34 ± 0.15	-0.34	-0.34	-0.29
k_3	$+0.03 \pm 0.02$	$+0.03$	$+0.03$	-
z_{peak}	2.56 ± 0.27	2.56	2.56	2.4
z range	$1 < z < 5$	$1 < z < 5$	$1 < z < 5$	$0.4 < z < 2.1$
Spectroscopic sample size	183	81	102	15,830

[a]Evolution parameters have been fixed for the red and blue subsamples.

[b]2QZ z_{peak} value is an extrapolation of the evolution of the $0.4 < z < 2.1$ luminosity function.

TABLE 3
BINNED $1/V_{max}$ $z = 2$ QUASAR LUMINOSITY FUNCTION

8 μm absolute magnitude range	Space Density at $z = 2$ (Mpc^{-3}mag^{-1})[a]	
	$1.0 < z < 5.0$ Quasars	$1.5 < z < 2.5$ Quasars
$-27.4 < M_8 < -27.0$	$4.3 \pm 1.0 \times 10^{-6}$	-
$-27.8 < M_8 < -27.4$	$2.4 \pm 0.5 \times 10^{-6}$	-
$-28.2 < M_8 < -27.8$	$3.0 \pm 0.4 \times 10^{-6}$	$2.4 \pm 0.6 \times 10^{-6}$
$-28.6 < M_8 < -28.2$	$1.2 \pm 0.2 \times 10^{-6}$	$1.1 \pm 0.2 \times 10^{-6}$
$-29.0 < M_8 < -28.6$	$6.1 \pm 0.9 \times 10^{-7}$	$4.5 \pm 1.0 \times 10^{-7}$
$-29.4 < M_8 < -29.0$	$2.6 \pm 0.5 \times 10^{-7}$	$2.7 \pm 0.7 \times 10^{-7}$
$-29.8 < M_8 < -29.4$	$2.4 \pm 0.5 \times 10^{-7}$	$2.0 \pm 0.6 \times 10^{-7}$
$-30.2 < M_8 < -29.8$	$9.2 \pm 2.4 \times 10^{-8}$	$6.8 \pm 2.5 \times 10^{-7}$
$-30.6 < M_8 < -30.2$	$4.7 \pm 1.5 \times 10^{-8}$	$7.4 \pm 2.8 \times 10^{-8}$
$-31.0 < M_8 < -30.6$	$< 7.2 \times 10^{-8}$	$< 2.8 \times 10^{-7}$
$-31.4 < M_8 < -31.0$	$2.3 \pm 0.9 \times 10^{-8}$	$4.9 \pm 2.1 \times 10^{-8}$

[a]Upper limits are 3σ.